A deglaciation model of the Oberhasli, Switzerland

Article *in* Journal of Quaternary Science · January 2016

DOI: 10.1002/jqs.2831

6 authors, including:

Jerzy Zasadni
AGH University of Science and Technology i…
33 PUBLICATIONS **83** CITATIONS
SEE PROFILE

Marcus Christl
ETH Zurich
140 PUBLICATIONS **1,909** CITATIONS
SEE PROFILE

Florian Kober
NAGRA
79 PUBLICATIONS **704** CITATIONS
SEE PROFILE

Christian Schlüchter
Universität Bern
158 PUBLICATIONS **4,619** CITATIONS
SEE PROFILE

 ISSN 0267-8179. DOI: 10.1002/jqs.2831

A deglaciation model of the Oberhasli, Switzerland

CHRISTIAN WIRSIG,[1]* JERZY ZASADNI,[2] SUSAN IVY-OCHS,[1] MARCUS CHRISTL,[1] FLORIAN KOBER[3] and CHRISTIAN SCHLÜCHTER[4]
[1]Laboratory of Ion Beam Physics, ETH Zürich, Switzerland
[2]Faculty of Geology, Geophysics and Environmental Protection, AGH University of Science and Technology, Kraków, Poland
[3]Geology, ETH Zürich, Switzerland
[4]Geology, University of Bern, Switzerland

Received 9 March 2015; Revised 6 November 2015; Accepted 9 December 2015

ABSTRACT: We combine ^{10}Be surface exposure ages from boulders and bedrock, field observations and measurement of bedrock ice-flow direction indicators with numerical ice surface models to develop a model of the evolution of the Oberhasli area in the central Swiss Alps from the Last Glacial Maximum (LGM) to the early Holocene. Surface exposure ages from bedrock and boulder samples imply that the highest ice surface at the glacial trimline in Haslital was attained at 23.0 ± 0.8 ka. Significant retreat followed no later than 17.7 ± 0.8 ka. Several boulders were let down on the Gelmerhörner ridge during lowering of the ice surface of the Aare LGM glacier. Their exposure ages of 16–14 ka suggest that patches of remnant ice persisted on the trough shoulder until the Bølling–Allerød interstadial. Lateglacial glacier systems in the High Alps were of a dendritic character, confined to the trunk valleys and cirques. Based on combined evidence from glacial erosional marks, surface exposure ages and numerical modelling we have been able to constrain the likely terminal position and ice surface of the Egesen stadial glacier (Younger Dryas equivalent) in Haslital. Exposure ages from the trough floor imply that deglaciation was completed at the end of the Younger Dryas at 12.2–10.8 ka. Copyright © 2016 John Wiley & Sons, Ltd.

KEYWORDS: ^{10}Be; deglaciation history; exposure dating; Haslital; High Alps.

Introduction

The stratigraphic framework of glaciations on the continents has been constructed based on the mapping and dating of moraines and other glacial sediments. This allowed constraints on the timing and extent of terrestrial glaciations during the global Last Glacial Maximum (LGM) (Ehlers *et al.*, 2011, and references therein). In the Alps, surface exposure dating and radiocarbon dating in both the northern and the southern forelands have shown that Alpine piedmont lobes exhibit a similar temporal distribution to the global LGM (Ivy-Ochs, 2015). Based on radiocarbon dating and pollen analysis in the Tagliamento amphitheatre, Monegato *et al.* (2007) showed that the Tagliamento glacier reached its maximum LGM position in a first pulse between 26.5 and 23 ka. It then retreated and readvanced to a similar extent during a second culmination phase and remained there until 19 ka. Similarly, piedmont lobes in Italy and in the northern Alpine foreland had abandoned their outermost LGM positions by no later than 24 ka (Ivy-Ochs *et al.*, 2004; Gianotti *et al.*, 2008, 2015; Akçar *et al.*, 2011; Reuther *et al.*, 2011; Federici *et al.*, 2012; Ravazzi *et al.*, 2014; Reber *et al.*, 2014; Ivy-Ochs, 2015). By no later than 19–18 ka, ice had completely disappeared from the northern forelands and had withdrawn to behind the mountain front (Lister, 1988; van Husen, 1997; Reitner, 2007; Ivy-Ochs *et al.*, 2008).

A series of Lateglacial stadials is observed across the Alps, with glaciers readvancing into ice-free mountain valleys (Penck and Brückner, 1901/9; Mayr and Heuberger, 1968; Kerschner and Berktold, 1982; Maisch, 1982; van Husen, 1997). The Gschnitz readvance is dated to 17–16 ka (Ivy-Ochs *et al.*, 2006a, recalculated, see below) and the Egesen stadial to 13.0–11.5 ka (Ivy-Ochs *et al.*, 2009; Schindelwig *et al.*, 2012, recalculated). The Gschnitz and Egesen readvances may be related to the two most significant climatic deteriorations of Termination 1, Heinrich event 1 at ~16.8 ka and the Younger Dryas at 12.9–11.5 ka (Bond *et al.*, 1992; Clark *et al.*, 2012). By around 10 ka glaciers had retreated to their Little Ice Age (LIA) extent or smaller (Ivy-Ochs *et al.*, 2009; Solomina *et al.*, 2015).

Glaciers leave a record of their past presence not only in moraines but in the bedrock as well. This evidence comprises glacial striae and trimlines, among other features (Glasser and Bennett, 2004). The glacial trimline defines the upper limit of ice-sculpted bedrock (Thorp, 1981). The smooth and rounded morphology below the trimline evidences pronounced glacial erosion in contrast to the jagged rock above the trimline marked by frost-shattering. The trimline in the Alps is interpreted to represent the maximum elevation of the active ice surface during the LGM (Penck and Brückner, 1901/9; Jäckli, 1962; van Husen, 1987). Although there may have been patches of cold-based ice early in the LGM, in the Alps there is no geomorphological evidence for a persistent thermal boundary as has been discussed, for example, for the Fennoscandian ice sheet (Fabel *et al.*, 2002). In addition to trimline evidence, the LGM ice surface was reconstructed based on the locations of high-elevation erratics as well as ice-flow direction indicators, such as striae, crescentic gouges and rat tails (Jäckli, 1962; van Husen, 1987; Florineth and Schlüchter, 1998; Kelly *et al.*, 2004; Bini *et al.*, 2009). The latter allowed the identification of several ice dispersal centres within the Alpine ice cap, for example the Rhône ice dome, which in turn fed piedmont glaciers in the foreland (Bini *et al.*, 2009).

In contrast to the wealth of information on the timing and extent of the piedmont lobes in the northern Alpine foreland (Ivy-Ochs *et al.*, 2008; Preusser *et al.*, 2011; Ivy-Ochs, 2015), appreciably less is known about the chronology of deglaciation in the High Alps (Kelly *et al.*, 2006; Dielforder and Hetzel, 2014; Hippe *et al.*, 2014). Considering the inertia of the gigantic masses of LGM ice located in the Alps, it cannot simply be assumed that ice in the High Alps disappeared at the same time as the comparably thin piedmont lobes at lower altitudes. In addition, Lateglacial stadial extents are difficult to constrain in areas where moraines are not present or have been buried by Holocene deposits. To address these questions,

*Correspondence: C. Wirsig, as above.
E-mail: wirsig@phys.ethz.ch

we present a detailed study on the mode and timing of the step-wise deglaciation of the Oberhasli valley system in the central Swiss Alps (Fig. 1). Based on field observations in combination with surface exposure dating and ice surface models, we reconstruct the distribution of ice masses and flow directions at several stages of the deglaciation process. This allows us to gain insight into the chronology and pattern of ice decay at a central location in the High Alps.

Setting

The Oberhasli is located in canton Bern at the centre of the Swiss Alps. Its major valley, Haslital, is traversed by the Aare River and stretches from Grimsel Pass at an elevation of 2164 m to Meiringen (595 m) (Fig. 1). The valley section to the south of Innertkirchen belongs to the Aarmassif, a part of the crystalline basement of the Helvetic zone of the Alps (Labhart, 1977; Abrecht, 1994). Here mainly granitic or gneissic rocks form steep walls on both sides of the deep trough valley. The study area around Gelmersee almost exclusively encompasses lithologies of Aare granite (Labhart, 1977; Abrecht, 1994). Due to this highly weathering-resistant framework the area is one of the best places in the Alps to study classic glacial erosional morphology. Large-scale features such as the U-shape of Haslital with impressive trough walls, pronounced trough shoulders and glacial trimlines are as well preserved as small-scale glacial polish and striae. Hanging valleys to the east and west join at several hundred metres above the valley floor (Fig. 2).

During the LGM Haslital was occupied by the Aare glacier that extended beyond Bern where it joined the northern lobe of the Rhône glacier (Penck and Brückner, 1901/9; Jäckli, 1962; Bini *et al.*, 2009). Only the highest peaks stood above the ice that filled the valley with a thickness of more than 1000 m. The glacier was supported not only by local accumulation areas in the tributary valleys, but was additionally fed from the Rhône ice dome once the latter had built up sufficiently to flow across Grimsel Pass (Fig. 1; Florineth and Schlüchter, 1998). The elevation of the ice surface in Haslital thus depended strongly on the contribution of large ice volumes from the Rhône ice dome. However, due to the high altitude of the pass (2164 m), this transfluence configuration was active only during phases of maximum glaciation (Ivy-Ochs, 1996; Florineth and Schlüchter, 1998; Kelly *et al.*, 2006).

While the contour of the ice surface during the LGM is well depicted in the trimlines, unequivocal indications of the extent of Lateglacial readvances observed elsewhere in the Alps are missing in Oberhasli. Hantke (1980, 2011) discusses an end moraine at the electricity plant at Handegg (Fig. 1) and attributes it to the Egesen stadial. He further identifies moraines at Meiringen (Hantke, 1980) that he attributes to the Gschnitz stadial readvance (Hantke, 2011).

Gelmer valley is the southernmost hanging valley on the east side of Haslital, roughly 6 km from Grimsel Pass. It hosts a hydropower reservoir, Gelmersee, that is connected to the small village of Handegg by Europe's steepest funicular. At the northern shoreline of Gelmersee, the Gelmerhörner ridge

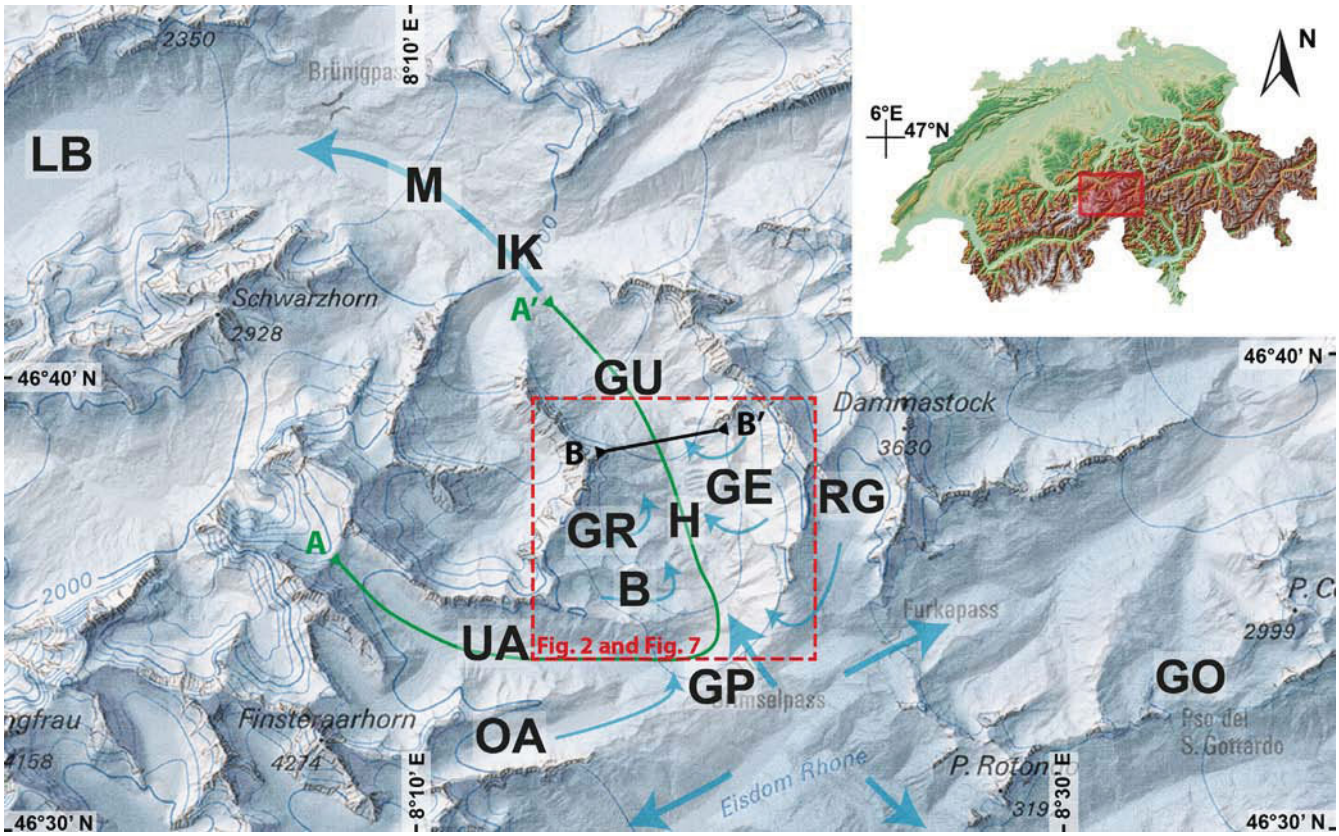

Figure 1. Modified excerpt from Bini *et al.* (2009) on top of a hillshade model showing a reconstruction of the study area in the central Swiss Alps during the LGM and locations mentioned in the text. The inset shows the position within Switzerland. The red box marks the extent shown in Figs 2 and 7. The blue arrows indicate the direction of ice flow. The LGM Aare glacier was fed by transfluence from the Rhône ice dome over Grimsel Pass and contributions from the Rhône, Unteraar and Oberaar glaciers and from Haslital's tributary valleys. The green line AA′ is the line of the profile in Fig. 8. The black line B–B′ is the line of profiles in Fig. 6. B = Bächli valley, GE = Gelmersee, GO = Gotthard Pass, GP = Grimsel Pass, GR = Grueben cirque, GU = Guttannen, H = Handegg, IK = Innertkirchen, LB = Lake Brienz, M = Meiringen, OA = Oberaar glacier, RG = Rhône glacier, UA = Unteraar glacier, W = Willigen. Hillshade model based on swissALTI3D DEM reproduced by permission of swisstopo (JA100120).

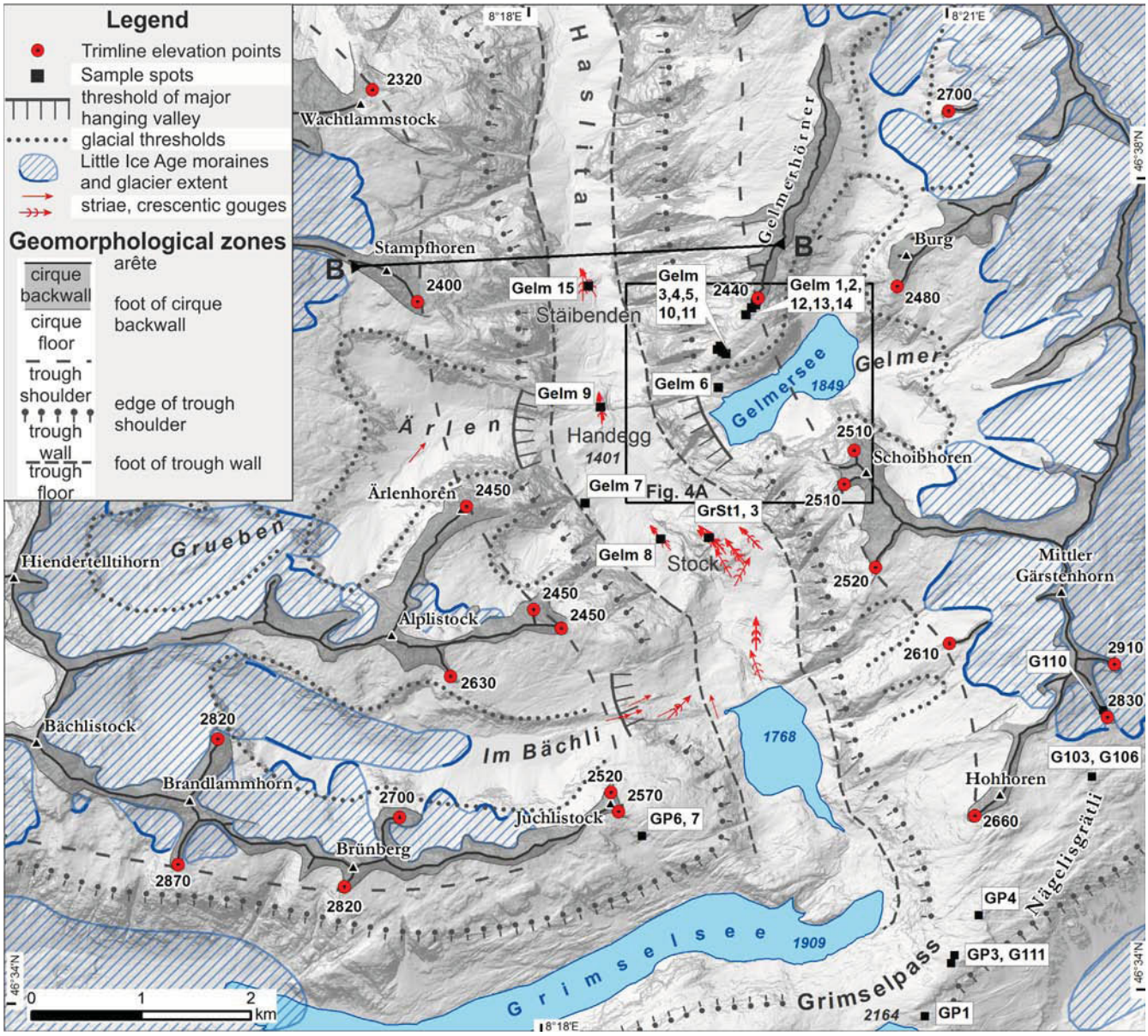

Figure 2. Simplified geomorphological map of the study region with sample locations, location and direction of glacial erosional marks and trimline points. Black box indicates extent of Fig. 4A, the black line BB′ is the line of profiles in Fig. 6. Hillshade model in background based on swissALTI3D DEM reproduced by permission of swisstopo (JA100120).

rises in the form of an almost vertical, 260-m-high trough wall within the tributary valley (Fig. 3A). Its smoothly abraded bedrock surface of the southern slope is in contrast to the craggy drop facing north. The ridge to some extent has a roche moutonnée shape, a clear sign that it was overridden by the LGM Aare glacier. The area is a popular place for hiking and mountaineering, well-known for slab climbing on the glacially polished granite walls. Many of its cirques remain occupied by small glaciers above 2600–2800 m that have receded considerably compared with their maximum Holocene extension at the end of the LIA (ca. 1850) (Fig. 2; Maisch *et al.*, 1999).

Methods

Field methods

Grinding of material transported at the base of the glacier on a bedrock surface produces linear scratches, or sometimes arc-shaped indentations (Agassiz, 1838) whose directions are used to infer palaeo-ice-flow directions (Florineth and Schlüchter, 1998; Glasser and Bennett, 2004; Benn and Evans, 2010). We mapped all such ice-flow direction indicators over an area of ca. 20 km^2 focusing on the Haslital trough walls, the spots where tributary valleys join the main valley and bedrock outcrops on the valley floor. We took orientation measurements of glacial striae and series of crescentic gouges (Fig. 3D). We did not record single crescentic gouges, because of the ambiguity of the indicated direction. Series of crescentic gouges, however, were taken as evidence of past ice-flow direction, in contrast to striae records that only indicate orientations. Where thin and shallow striae cross-cut crescentic gouges or deeper striae of an older generation, both orientations were noted and assigned to different palaeo-glacier advances that moved past the same location, but in a different direction.

We register trimline elevation points exclusively at the ends of truncated spurs. To account for the uncertainty in the record and method, we report a maximum and minimum elevation for each trimline elevation point, defined as the lowest point of the arête and the break in slope at the

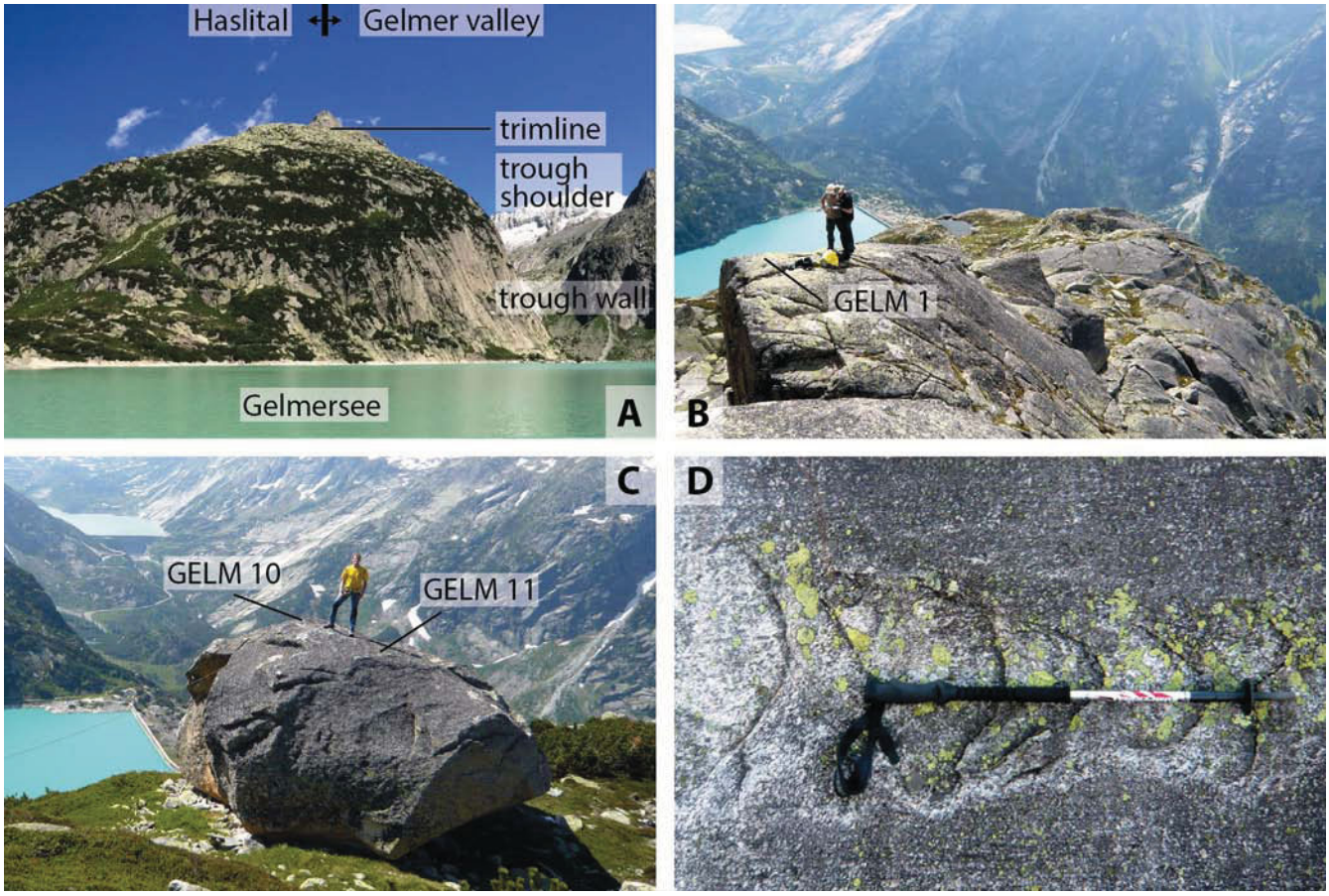

Figure 3. Representative pictures showing: (A) view of Gelmerhörner ridge as seen from the Gelmersee southern shore illustrating the general position of geomorphological zones. The difference in elevation between the lake and the trimline is ~ 600 m. (B) GELM1, polished bedrock in a very exposed position at the Gelmerhörner trimline. (C) GELM10/11, a 14 × 10 × 5-m boulder (L×W×H) on the trough shoulder. (D) Crescentic gouges at Gelmersee. The hiking pole (~1 m) points in the inferred direction of palaeo ice flow.

transition to the trough shoulder zone, respectively. This large-scale morphology approach has the advantage that it can be performed remotely, i.e. by a combination of field observations and usage of Digital Elevation Models (DEMs).

Ice surface reconstruction

The LGM ice surface is reconstructed in GIS in two steps: first, in the trunk valley the ice surface is defined by the trimline elevation points. The objective is to achieve an average consistent slope within the limits of uncertainty. If possible, the reconstruction follows the maximum elevation of each trimline elevation point rather than the minimum. Second, the ice surface is coherently extended to the top of the cirque backwalls in the tributary valleys, taking ice-flow directions inferred from erosional marks into account.

The GIS reconstructions of Lateglacial stadials are chiefly constrained by surface exposure ages and ice-flow direction indicators (see also below). In addition, we employ an ice surface model (Benn and Hulton, 2010) that calculates valley shape factors and ice thickness with a given glacier bed and shear stress. The former glacier bed (bedrock surface) along the modelled profile path (green line in Fig. 1) is represented by the swissALTI3D DEM combined with bathymetry data from topographic maps to reconstruct bedrock beneath lakes. Underneath the Unteraar glacier, the bedrock floor is modelled using the ice thickness calculated by Farinotti *et al.* (2009). The palaeo-Aare glacier is modelled as a single large valley glacier; the contributions from glaciers coming in from the tributary valleys are not taken into account. Shear stress is confined to the range of realistic values of 50–150 kPa (Cuffey and Paterson, 2010, p. 54f). The ice surface modelled from potential terminal positions is tested against field evidence for the palaeo-ice surface to identify realistic scenarios.

^{10}Be surface exposure dating

Rock samples were collected in 2013 (GrSt1,3 in 2006) from the top surface of boulders, where available, and otherwise from bedrock. All selected boulders are sufficiently tall (> 1 m) and rest in a stable position, rendering post-depositional movement unlikely (Akcar *et al.*, 2011). Quartz veins with preserved glacial polish protruding from the surface indicate < 2 cm of erosion. Samples of 0.5–4.0 cm thickness were taken with hammer and chisel at the highest point of the regular boulder surface, avoiding sharp edges. Much care was taken in the selection of bedrock sample locations, as they are prone to be affected by temporary cover of sediments, ice or snow. Ideal locations were identified on the highest points of roche moutonnée features, nearby steep drops of several metres, but staying clear from the zone of glacial plucking. The preserved smooth surface, at some spots still glacially polished, indicates negligible postglacial erosion. Representative samples are portrayed in Fig. 3(B,C).

We selected three distinct geomorphological units for sample collection to address separate research questions: trimline, trough shoulder and trough floor. The first two groups are from two different elevation ranges on the Gelmerhörner ridge. Samples from the trimline zone were collected to date the onset of initial decay of the LGM ice surface in Haslital: three bedrock surfaces just beneath the glacial trimline at 2410–2440 m (GELM1,2,12) and a boulder

and another bedrock surface further downhill at 2369/2334 m (GELM13,14), referred to as 'trimline samples'. Further downhill, at the middle of the trough shoulder (Fig. 2) is a comparably flat (slope $< 20°$) and broad area between 2080 and 2200 m, partially covered by low-growing vegetation. Here we took samples of three boulders (GELM3,4,10/11) and of one bedrock surface (GELM5). From these 'trough shoulder samples' we anticipated insight into the rate of ice surface lowering and the mode of ice decay in Haslital. At the trough floor, the third unit, four samples were taken on exposed outcrops of glacially polished bedrock in Haslital (GELM7,8,9,15) plus one from the bedrock floor of Gelmer valley (GELM6) (Fig. 2). Two additional samples (GrSt1,3) originate from the top of Stock, a more than 100-m-high bedrock hill positioned in the centre of the Haslital valley floor. While GrSt3 is from an outcrop of bedrock, GrSt1 is taken from the weathered surface of a boulder. These 'trough floor samples' were intended to provide information on the extent and timing of Lateglacial readvances in Haslital.

Beryllium sample preparation follows the method of Kohl and Nishiizumi (1992) and is described in detail by Ivy-Ochs *et al.* (2006b). The collected rock was first crushed and sieved to grain sizes < 1 mm. After separating the quartz in HCl and diluted HF, a ^{9}Be carrier was added and the quartz dissolved in HF. Be was purified using ion exchange columns and selective precipitation. Accelerator mass spectrometry (AMS) measurements of ^{10}Be/^{9}Be were carried out on the 600 kV TANDY system (Christl *et al.*, 2013) at the Laboratory of Ion Beam Physics (LIP) at ETH Zürich. The measured ratios were normalized to the ETH Zürich in-house standard S2007N which in turn was calibrated relative to the 07KNSTD standard (Nishiizumi *et al.*, 2007). GrSt1 and 3 were measured against the S555 standard. ^{10}Be/^{9}Be ratios were corrected with long-term average full chemistry procedural blanks of $(3.6 \pm 2.6) \times 10^{-15}$. Ages were calculated using the CRONUS-EARTH online calculator (Balco *et al.*, 2008) with a sea-level high-latitude (SLHL) production rate of 3.87 ± 0.19 at g^{-1} a^{-1} originally established for north-east North America ('NENA', 'Lm' scaling, Balco *et al.* (2009)), but showing excellent agreement with many recently published production rate calibrations worldwide (Fenton *et al.*, 2011; Briner *et al.*, 2012; Goehring *et al.*, 2012; Putnam *et al.*, 2012; Young *et al.*, 2013; Claude *et al.*, 2014; Heyman, 2014) using the 'Lm' scaling theme (Lal, 1991; Balco *et al.*, 2008). Accounting for the observed differences in surface weathering, an erosion rate of 0.1 mm ka^{-1} was used for bedrock and 1 mm ka^{-1} for boulder samples. Stated internal errors (1σ) include AMS standard reproducibility, counting statistics, standard mean error of samples and uncertainty of the blank correction ('int.' in Table 3). Reported external errors ('ext.' in Table 3) additionally propagate the uncertainty of the local production rate.

We applied a correction for snow cover to all bedrock samples but not to those at the highest trimline (GELM1,2,12) or boulders based on the following reasoning (Hippe *et al.*, 2014). The closest weather station at Grimsel Hospiz (1970 m) records a snow cover of more than 1 m for 6 months and a maximum of 280 cm in April on average over the last 65 years (www.wsl.ch, Eidgenössische Forschungsanstalt für Wald, Schnee und Landschaft WSL). It is difficult to say, however, how well the modern dataset represents the entire exposure history of our samples including drastic climatic shifts during the Lateglacial and Holocene. We particularly selected exposed sample sites on the ridge crest where local topography and exposure to intense wind strongly impede accumulation of snow or ice. In particular, GELM1,2,12 come from very narrow and steep terrain that offers no place for snow accumulation (Fig. 3B). Visual observations conducted in the springs of 2013–2015 demonstrate that the parts of the ridge crest that we sampled remain snow-free. For the trough floor bedrock samples, the careful selection of sample sites at the top of cross-valley bedrock ridges (GELM9, 15) or at steep, glacially polished slopes (GELM7, 8) implies limited accumulation of annual snow. We therefore apply a snow correction of 50 cm for 6 months, which is less than today's measured values. It is estimated following eq. 3.76 in Gosse and Phillips (2001) with a snow density of 0.3 g cm^{-3} and an attenuation length for fast neutrons in snow of 109 g cm^{-2} (Zweck *et al.*, 2013; Delunel *et al.*, 2014; Dunai *et al.*, 2014) considering only the effect on spallogenic production (cf. Schildgen *et al.*, 2005) to $S_{snow,max} = 0.936$.

Mapping results

The weathering-resistant granitic lithologies found in Oberhasli preserve glacial erosional features efficiently for long periods. Glacial polish and striae are ubiquitously encountered wherever bedrock is exposed in the valley. Detailed direction measurements were made on the Gelmerhörner ridge, at the mouth of Gelmer and Bächli valley and along the Haslital valley floor.

On the Gelmerhörner ridge the direction gradually shifts from SW to NW with decreasing elevation and proximity to Haslital. On the top of the bedrock step at the mouth of Gelmer valley we distinguish three distinct generations of glacial marks. The oldest one points NW-N, parallel to the trunk valley (Fig. 4A, blue symbols). The second generation is distinguished from the first by some crosscutting situations, clearly showing they were formed at different points in time. It is mainly orientated westwards, almost perpendicular to the first generation, but gradually shifts towards NW with proximity to Haslital (Fig. 4B, green symbols). The youngest set mostly consists of striations and shallow marks that crosscut the deeper marks of the second generation. It indicates straight downhill W-SW movement transverse to the trunk valley (Fig. 4B, red symbols). Preservation of the older erosional features signifies a locally weak erosive capability of the readvancing glacier, constrained by the original depth of old-generation striae or crescentic gouges of a few centimeters.

Striae and crescentic gouges at Im Bächli indicate straight downhill E-NE ice-flow exiting the tributary valley (Fig. 2). Below an altitude of ~1920 m, however, glacial erosional marks exclusively point NNE, following the direction of the palaeo-Aare glacier in Haslital. On the Haslital valley floor, the dominant orientation of striae and crescentic gauges follows the course of the main valley: NNW between Grimsel Pass and Stock, NW on stock and N to the north of Stock.

Detected trimline elevation points are listed in Table 1. Elevations range from 2780 m at Gärstenhörner to 2450 m at Alplistock, generally decreasing coming from the tributary valleys into the main trough and going northwards from Grimsel Pass down Haslital.

Modelling results

Valley shape factors for Gschnitz and Egesen palaeo-glaciers calculated along the modelled profile (red line in Fig. 3) of 0.5–0.6 are in the normal range for deeply incised, narrow alpine valleys (Cuffey and Paterson, 2010). The ice surface was modelled with numerous candidates for Lateglacial terminal positions as remote as Interlaken at Lake Brienz, ~45 km downvalley from Handegg. As Lateglacial stadials across the Alps were confined to inner-Alpine valleys

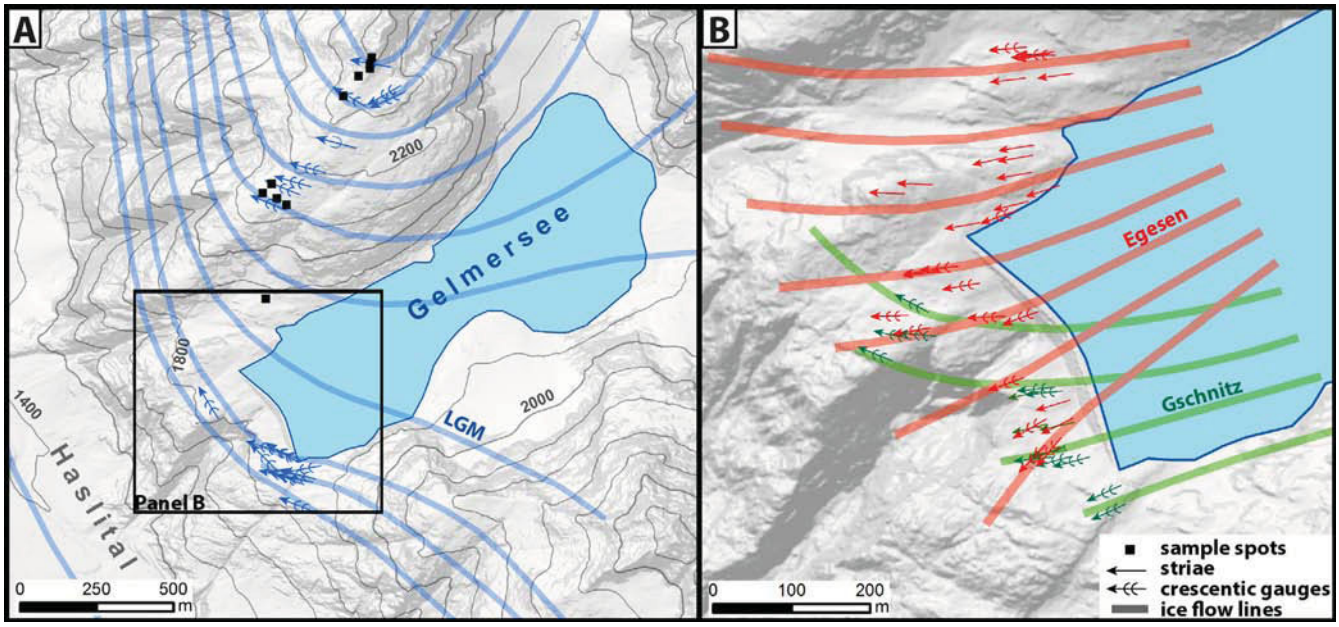

Figure 4. (A) Sample locations, directions of glacial erosional marks of first-generation (LGM, blue) and deduced ice-flow lines around Gelmersee. Black box indicates extent of panel B. (B) Details of bedrock in front of Gelmersee dam showing glacial erosional marks of the second (Gschnitz, green) and third (Egesen, red) generation and deduced ice flow lines. Hillshade model in background based on swissALTI3D DEM reproduced by permission of swisstopo (JA100120).

(Ivy-Ochs *et al.*, 2008) this can be considered a conservative maximum extent. The modelled ice surface still remains below the sampling sites on the trough shoulder for all terminus candidates and shear stress $\leq$ 150 kPa. The position of lateral moraines on the southern side of Grimsel Pass attributed to Lateglacial stadials (Hantke, 1980) indicates that transfluence of the Rhône glacier can be neglected. This is confirmed by our modelled Egesen Aare glacier that neither reaches the elevations of Grimsel Pass, nor the mouth of Gelmer valley with a terminal position anywhere between Guttannen and Handegg.

Table 1. List of trimline elevation points.

Location	Latitude	Longitude	Elevation (m)	
	WGS84		Max.	Min.
Alplistock E (1)	46.5955	8.3022	2450	2390
Alplistock E (2)	46.5970	8.2989	2450	2380
Alplistock SE	46.5916	8.2889	2630	2580
Ärlenhoren	46.6055	8.2910	2450	2425
Brandlammhorn N	46.5866	8.2611	2820	2780
Brandlammhorn S	46.5764	8.2563	2870	2800
Brünberg N	46.5801	8.2827	2700	2660
Brünberg S	46.5744	8.2760	2820	2740
Burg	46.6232	8.3426	2480	2420
Diechterlimi SW	46.6375	8.3490	2700	2670
Gelmerhörner S	46.6224	8.3260	2440	2410
Hohhoren	46.5797	8.3511	2660	2620
Juchlistock N	46.5819	8.3078	2520	2470
Juchlistock S	46.5803	8.3087	2570	2530
Mittler Gärstenhorn W	46.5939	8.3483	2610	2580
Schoibhoren N	46.6098	8.3372	2510	2470
Schoibhoren W	46.6070	8.3360	2510	2480
Stampfhoren	46.6224	8.2855	2400	2300
Tafelgrätli W	46.6002	8.3396	2520	2500
Vorder Gärstenhorn E	46.5920	8.3679	2910	2810
Vorder Gärstenhorn S	46.5876	8.3670	2830	2780
Wachtlammstock	46.6398	8.2804	2320	2290

Dating results

Sample information and measured ^{10}Be concentrations are listed in Table 2. Table 3 summarizes calculated exposure ages and uncertainties at the 1σ level. It further includes values of samples from Grimsel Pass published by Ivy-Ochs (1996) and Kelly *et al.* (2006), here recalculated for homogeneity with the NENA ^{10}Be production rate. Figure 5 gives an overview of obtained ages on the Gelmerhörner ridge.

The obtained ages range from 10.8 $\pm$ 0.8 to 23.1 $\pm$ 1.6 ka. We refer to ages including snow shielding, where applicable. The age distribution varies considerably between different geomorphological units. The oldest surfaces are encountered at the Gelmerhörner LGM trimline where we dated five samples. Here the two surfaces at the highest elevation (GELM2,12) yield exposure ages of approximately 23.0 ka. The three remaining trimline samples were exposed for 17.7–16.3 ka. At the trough shoulder, the obtained ages from five samples are generally younger and range from 16.1 to 13.6 ka (Fig. 5). GELM10 and 11 were collected from different places on the surface of the same boulder. The error-weighted mean age of this boulder is 14.0 $\pm$ 0.5 ka. The two samples from the top of Stock are 11.0 $\pm$ 1.2 versus 15.4 $\pm$ 1.4 ka for GrSt1 and GrSt3, respectively. GELM6, on the floor of Gelmer valley, is 10.8 $\pm$ 0.8 ka old. The four bedrock surfaces from the Haslital trough floor were exposed for 11.0–12.2 ka, roughly since the beginning of the Holocene.

Discussion

Based on the observations and measurement results listed above we present a model for the evolution of Haslital from full LGM conditions to the Lateglacial/Holocene transition. We identify three distinct stages with specific glacial configurations that are discussed independently (summarized in Fig. 6).

Last Glacial Maximum

At the height of the LGM the Oberhasli was almost entirely covered by ice, dominated by the Aare glacier that filled up

Table 2. Sample list and measured ^{10}Be concentrations.

Sample ID	Latitude	Longitude	Elevation (m a.s.l.)	Thickness (cm)	Topographic shielding factor	^{10}Be concentration* (10^5 at g^{-1})
	WGS84					
GELM1	46.6218	8.3257	2387	1.0	0.977	4.58 ± 0.21
GELM2	46.6219	8.3257	2393	1.0	0.983	6.09 ± 0.31
GELM3	46.6178	8.3221	2144	1.0	0.943	3.37 ± 0.16
GELM4	46.6182	8.3211	2145	1.0	0.988	3.27 ± 0.15
GELM5	46.6185	8.3215	2155	1.0	0.979	3.04 ± 0.14
GELM6	46.6151	8.3212	1888	4.0	0.934	1.73 ± 0.10
GELM7	46.6057	8.3052	1534	2.0	0.883	1.43 ± 0.15
GELM8	46.6027	8.3141	1522	0.5	0.936	1.39 ± 0.12
GELM9	46.6136	8.3071	1418	1.0	0.949	1.39 ± 0.11
GELM10	46.6180	8.3217	2154	1.0	0.991	3.01 ± 0.12
GELM11	46.6180	8.3217	2154	1.0	0.986	3.17 ± 0.12
GELM12	46.6221	8.3258	2402	2.5	0.929	5.67 ± 0.26
GELM13	46.6216	8.3252	2369	1.0	0.957	4.03 ± 0.16
GELM14	46.6210	8.3246	2334	1.0	0.991	3.85 ± 0.11
GELM15	46.6238	8.3059	1316	1.0	0.915	1.14 ± 0.12
GrSt1	46.6027	8.3199	1727	2.0	0.956	1.87 ± 0.18
GrSt3	46.6027	8.3197	1725	2.0	0.952	2.45 ± 0.19

*GrSt1,3 measured against standard S555, all other samples measured against standard 07KNSTD (Nishiizumi *et al.*, 2007), corrected for full process blank of (3.6 ± 2.6)× 10^{-15} ^{10}Be/^{9}Be.

Table 3. Sample type, geomorphological unit and calculated exposure ages.

Sample ID	Elevation (m a.s.l.)	Type	Geomorphological unit	^{10}Be exposure age* (ka)			^{10}Be exposure age (ka) incl. snow corr.†	
				Age	± (int.)	± (ext.)	Age	± (ext.)
GELM12	2402	bedrock	trimline	22.9	1.1	1.5		
GELM2	2393	bedrock		23.1	1.2	1.6		
GELM1	2387	bedrock		17.7	0.8	1.2		
GELM13	2369	boulder, 1 m		16.0	0.6	1.0		
GELM14	2334	bedrock		15.4	0.4	0.9	16.4	0.9
GELM5	2155	bedrock	trough shoulder	13.9	0.7	0.9	14.8	1.0
GELM10	2154	boulder, 5 m		13.6	0.6	0.9		
GELM11				14.4	0.6	0.9		
GELM4	2145	boulder, 1 m		15.0	0.7	1.0		
GELM3	2144	boulder, 4 m		16.1	0.8	1.1		
GrSt1	1727	boulder	bedrock high on Haslital trough floor	11.0	1.1	1.2		
GrSt3	1725	bedrock		14.3	1.1	1.3	15.4	1.4
GELM6	1888	bedrock	Gelmer valley trough floor	10.2	0.6	0.8	10.8	0.8
GELM7	1534	bedrock	Haslital trough floor	11.4	1.2	1.3	12.2	1.4
GELM8	1522	bedrock		10.4	0.9	1.0	11.2	1.1
GELM9	1418	bedrock		11.2	0.9	1.0	12.0	1.1
GELM15	1316	bedrock		10.2	1.1	1.2	11.0	1.3
GP1‡	2230	bedrock	transfluence pass	12.4	0.5	0.8	13.2	0.8
G111§	2400	bedrock		13.7	1.1	1.3	14.5	1.4
GP3‡	2420	bedrock		15.1	1.3	1.5	16.1	1.6
GP4‡	2480	bedrock		15.3	0.8	1.1	16.4	1.2
GP6‡	2390	bedrock	cirque	13.2	0.7	1.0	14.1	1.0
GP7‡	2390	bedrock		11.4	0.5	0.8	12.2	0.8
G103§	2660	bedrock		11.1	0.8	1.0	11.9	1.1
G106§	2660	bedrock		10.3	0.8	0.9	11.0	1.0
G110§	2680	bedrock		11.9	0.9	1.1	12.7	1.1

*Using NENA production rates (3.87 ± 0.19) at g^{-1} a^{-1} (Balco *et al.*, 2009), 'Lm' scaling and erosion rates of 0.1 mm ka^{-1} for bedrock, 1 mm ka^{-1} for boulder samples. Rock density is 2.65 g cm^{-3}.
†Assuming 50 cm snow cover for 6 months per year.
‡Recalculated from Kelly *et al.* (2006).
§Recalculated from Ivy-Ochs (1996).

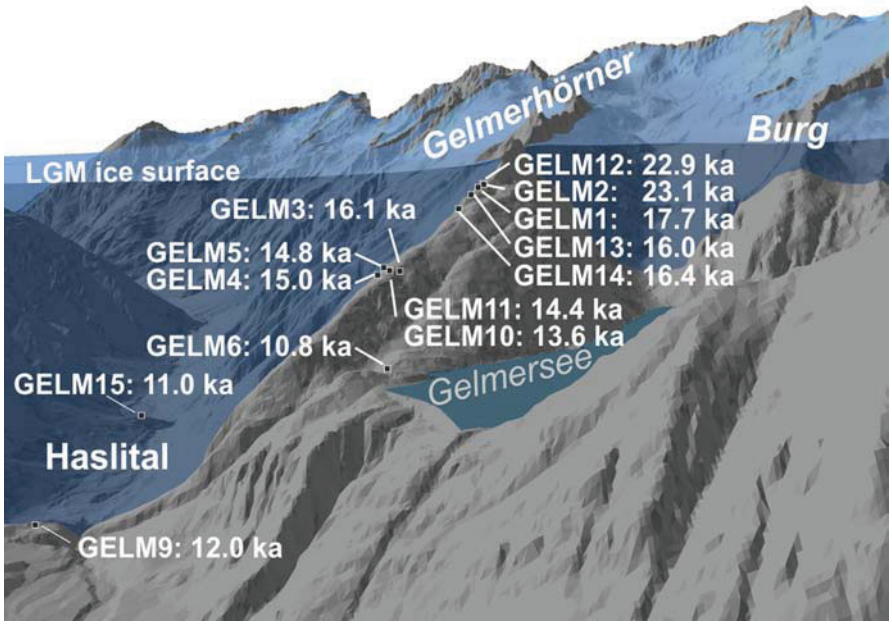

Figure 5. Overview of obtained exposure ages on the Gelmerhörner ridge and visible valley floor samples in relation to the reconstructed LGM ice surface. The oldest ages ~23 ka occur at the trimline (GELM2,12). The remaining ages on the ridge range from ~14 to 18 ka. Surfaces on the floor of Haslital and Gelmer valley are exposed for ~ 11–12 ka. Age uncertainties are listed in Table 3. Sample locations are superimposed on a landscape model based on the swissALTI3D DEM reproduced by permission of swisstopo (JA100120).

Haslital. The reconstruction of the ice surface presented in Fig. 7 is generally consistent with the geometry of earlier ones (Jäckli, 1962; Florineth and Schlüchter, 1998; Bini *et al.*, 2009; Fig. 1). The present reconstruction is constrained by a much denser network of trimline elevation points in comparison and therefore represents a more detailed model for the study area. During the LGM, the Oberhasli was situated in the accumulation area of the glacial system. Widespread glacial marks on the trough shoulder at Gelmerhörner ridge document the active subglacial erosion and therefore a warm-based palaeo-glacier, at least temporarily. Ice from the tributary valleys flowed into the main valley changing direction as it joined the Aare glacier. This is shown by the striations on the Gelmerhörner ridge that gradually shift direction from SW, out of the tributary valley, to NW, i.e. parallel to Haslital and the Aare glacier (Fig. 4A). The oldest generation of glacial erosional marks at the bedrock in front of Gelmersee are parallel to the trunk valley, and thus record dominant influence of the Aare glacier.

The two samples from the highest elevations, 10–50 m below the trimline (2410/2440 m at Gelmerhörner), represent this stage: GELM2 and 12. Their error-weighted mean age of 23.0 ± 0.8 ka does not overlap with any of the other trimline samples: GELM1 at the next highest location, 6 m below GELM2, yields an age of 17.7 ± 0.8 ka. We consider it highly unlikely that incomplete exposure of GELM1 can cause the discrepancy, because there is no place to accumulate more than a few centimetres of snow or ice at this site (Fig. 3B). Possibly, the apparent age discordance arises from excess nuclides that were inherited where subglacial erosion of the bedrock surfaces during the LGM was insufficient to completely remove the previously accumulated nuclide inventory. Indeed, the actual depths of erosion can vary significantly on a small spatial scale depending on, for example, bedrock lithology (Dühnforth *et al.*, 2010), local topography (Fabel *et al.*, 2004) and ice temperature (Fabel *et al.*, 2002; Stroeven *et al.*, 2002). As the samples located the closest to the glacial trimline were affected by relatively thin ice even during the LGM they perceivably received the least amount of erosion and consequently would show too old apparent exposure ages.

By contrast, it has been recognized that during the LGM culmination glacier ice margins in the Alps fluctuated significantly (e.g. Keller and Krayss, 2005; Monegato *et al.*, 2007). The glacial trimline then marks the highest elevation of an ice surface during the course of the LGM. Without evidence for differences in subglacial erosion between GELM1 and GELM2/12, it is possible that the oldest ages represent true exposure durations. In this case, the maximum glacial configuration was attained in the Oberhasli during the LGM buildup phase at ~23 ka BP, while subsequently the ice surface stayed slightly lower (Fig. 6A,B). This interpretation agrees well with results from the Tagliamento basin observing the most extensive LGM pulse at 26.5–23 ka BP and a second, slightly smaller culmination ending at 19 ka BP (Monegato *et al.*, 2007).

In both cases, the exposure age of GELM1 of 17.7 ± 0.8 ka, as the oldest age and highest elevated surface below GELM2 and 12, constitutes a robust minimum age for the onset of deglaciation (Fig. 7B). This is in excellent agreement with the recently determined age of initial ice downwasting of 18.0 ± 0.6 ka at Simplon pass (Dielforder and Hetzel, 2014). The fact that boulders were deposited in the LGM accumulation zone, close to the maximum ice surface (GELM13, 2369 m) and on the trough shoulder (GELM3,4,10/11, 2150 m) contains information on the mode of ice retreat. The placement of these boulders on the crest of the narrow ridge is not the result of a rock fall. They must have been deposited there by a glacier. Yet our models indicate that glaciers during the Lateglacial stadials did not reach this elevation of the Gelmerhörner ridge. Furthermore, there is no till on the ridge that would imply subglacial deposition and the preservation of a boulder the size of GELM10/11 ($14 \times 10 \times 5$m, Fig. 3C) during subglacial transport appears unlikely. Thus, these isolated boulders must have been let down during lowering of the LGM ice surface. Because it was demonstrated that the Gschnitz glacier readvanced into ice-free mountain valleys (van Husen, 1977) at 17–16 ka BP (Ivy-Ochs *et al.*, 2006a), most of the LGM ice must have melted previously. At Handegg in particular, the LGM ice surface downwasted from the trimline to below the level of the Aare Gschnitz ice surface (see next section), and therefore by at least 400 m within 1000–2000 years. The rapid disappearance of LGM ice might be explained by a small increase of the LGM equilibrium line altitude (ELA) that decreased the accumulation zone to a size that no longer

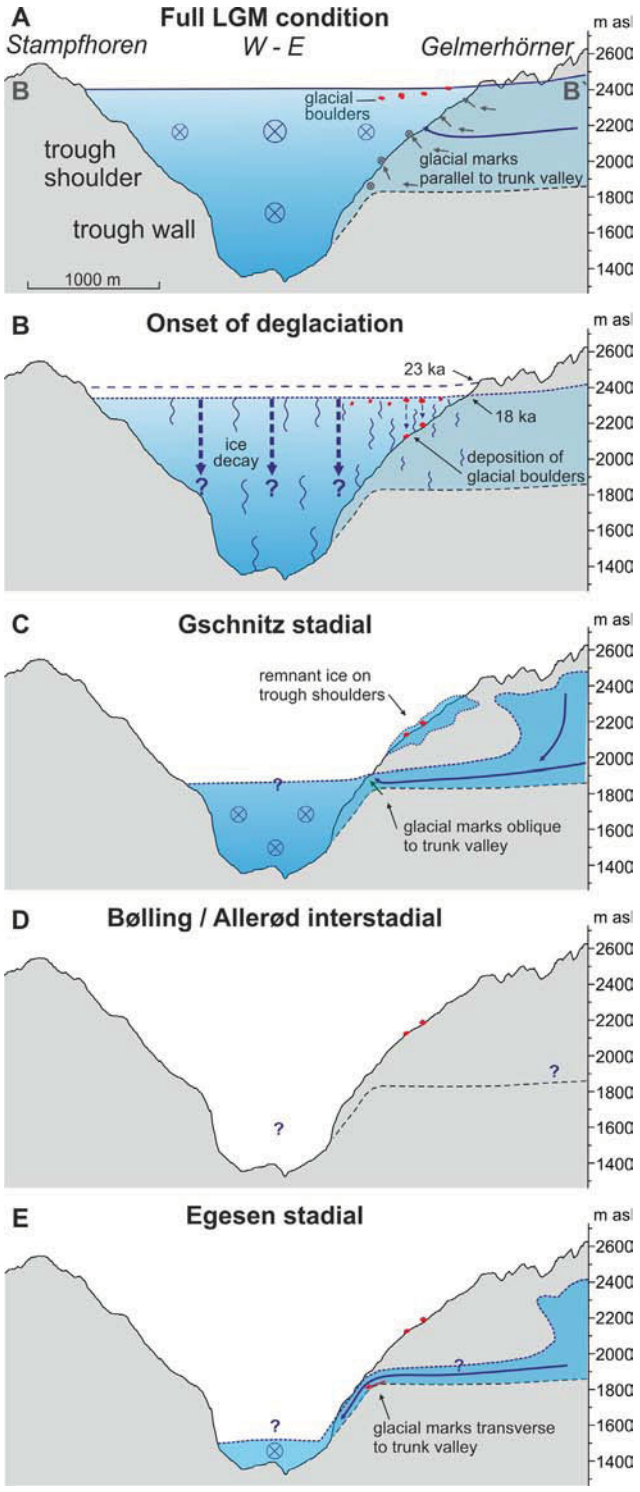

Figure 6. Illustration of the deglaciation model as a sequence of cross-valley profiles at five points in time between the LGM and Egesen stadial. (A) Full LGM condition: highest ice surface at ~23 ka. Ice accumulation throughout the Oberhasli and active ice flow to the north in Haslital. Supra- and/or englacial transport of glacial boulders. (B) Onset of deglaciation at ~18 ka: decay of the LGM ice. Glacial boulders let down on the trough shoulder during lowering of the LGM ice surface. (C) Gschnitz stadial (17–16 ka): trough and tributary cirques occupied by glaciers forming interconnected dendritic system. Remnant ice patches on trough shoulders. (D) Bølling–Allerød interstadial (14.7–12.9 ka): glaciers probably smaller than the Egesen glacier. Ice-free conditions on trough shoulders. (E) Egesen stadial (12.9–11.5 ka): dendritic glaciers confined to glacial troughs and cirques. Ice-free conditions on trough shoulders.

supported the extensive piedmont lobes in the Alpine foreland. When the ice surface thereupon declined, shear stress in the long, gently sloped piedmont lobes became low enough to significantly decrease the flow of ice and widespread ablation dominated.

The chronology of deglaciation in the northern Swiss Alpine foreland shows a similar pattern. Maximum positions were abandoned early: the Aare glacier at 21.5 ± 1.0 ka (Akcar *et al.*, 2011), the Reuss glacier at 22.2 ± 1.0 ka (Reber *et al.*, 2014) and the Rhône glacier at 24.3 ± 1.6 ka (Ivy-Ochs *et al.*, 2004, boulder ER2, recalculated). Just as reported here in Haslital, however, significant retreat followed later: at 18.6 ± 0.9 ka the Reuss glacier abandoned its frontal position at Wohlen, only 12 km from its maximum LGM extent (Reber *et al.*, 2014). Soon after, around 18 ka BP, lakes formed in the basins abandoned by the retreating piedmont lobes of the Rhône (Hadorn *et al.*, 2002) and Linth/Rhine glacier (Lister, 1988) and the northern Alpine foreland was completely free of ice (van Husen, 1997; Keller and Krayss, 2005; Ivy-Ochs *et al.*, 2008, and references therein). LGM ice surface lowering in Haslital appears to have followed shortly after or simultaneous with retreat from the terminal positions in the foreland.

Gschnitz Stadial

Despite the absence of moraines, we infer that Haslital was occupied during several Lateglacial stadials, echoing the pattern observed across the Alps (e.g. Mayr and Heuberger, 1968; Kerschner and Berktold, 1982; Maisch, 1982; van Husen, 1997). In contrast to the ice dome system during the LGM (Florineth and Schlüchter, 1998), early Lateglacial glaciers were of a dendritic character, confined by local topography, even though their exact dimensions in the central Swiss Alps are poorly known (Ivy-Ochs *et al.*, 2006a; Hantke, 2011). The glacial tongue in Haslital was sustained by contributions from all cirques in the tributary valleys of the area, including the catchment of today's Unter- and Oberaar glaciers, forming a large accumulation zone. We attribute the second generation of glacial erosional marks at Gelmersee (Fig. 4B, green symbols) to the most important early Lateglacial readvance, the Gschnitz stadial. The W-NW orientation indicates flow outbound of the tributary valley with marked influence from the main glacier in Haslital. To exert this deviation from the preferred downhill flow direction, the surface of the main glacier must have been as high or higher than the floor of the tributary Gelmer valley, which is at roughly 1800 m (Fig. 6C). The change in flow direction compared with the LGM indicates, however, that the Aare glacier was considerably smaller, i.e. the ice surface in Haslital was far lower than during the LGM. Yet, to further constrain the elevation of the Gschnitz ice surface we must rely on numerical modelling. Since the terminal position is also unknown we deployed several models with different end points. The Gschnitz ice surface in Haslital stayed below the trough shoulder on the Gelmerhörner ridge, however, even in the most conservative model with the terminal position at Lake Brienz (Fig. 1) and 150 kPa shear stress. Scenarios with a terminal position around Innertkirchen (cf. Beck, 1932) and 100–150 kPa shear stress conform best to the elevation and pattern of measured striations (Fig. 8).

Calculated surface exposure ages on the trough shoulder range from 13.6 to 16.1 ka (Fig. 5, GELM10 and 3). Our modelling indicates that the ice surface of the Aare glacier stayed below the sample locations on the trough shoulder throughout the Lateglacial. Furthermore, local topography inhibits local glaciers to cover the narrow ridge. The boulders

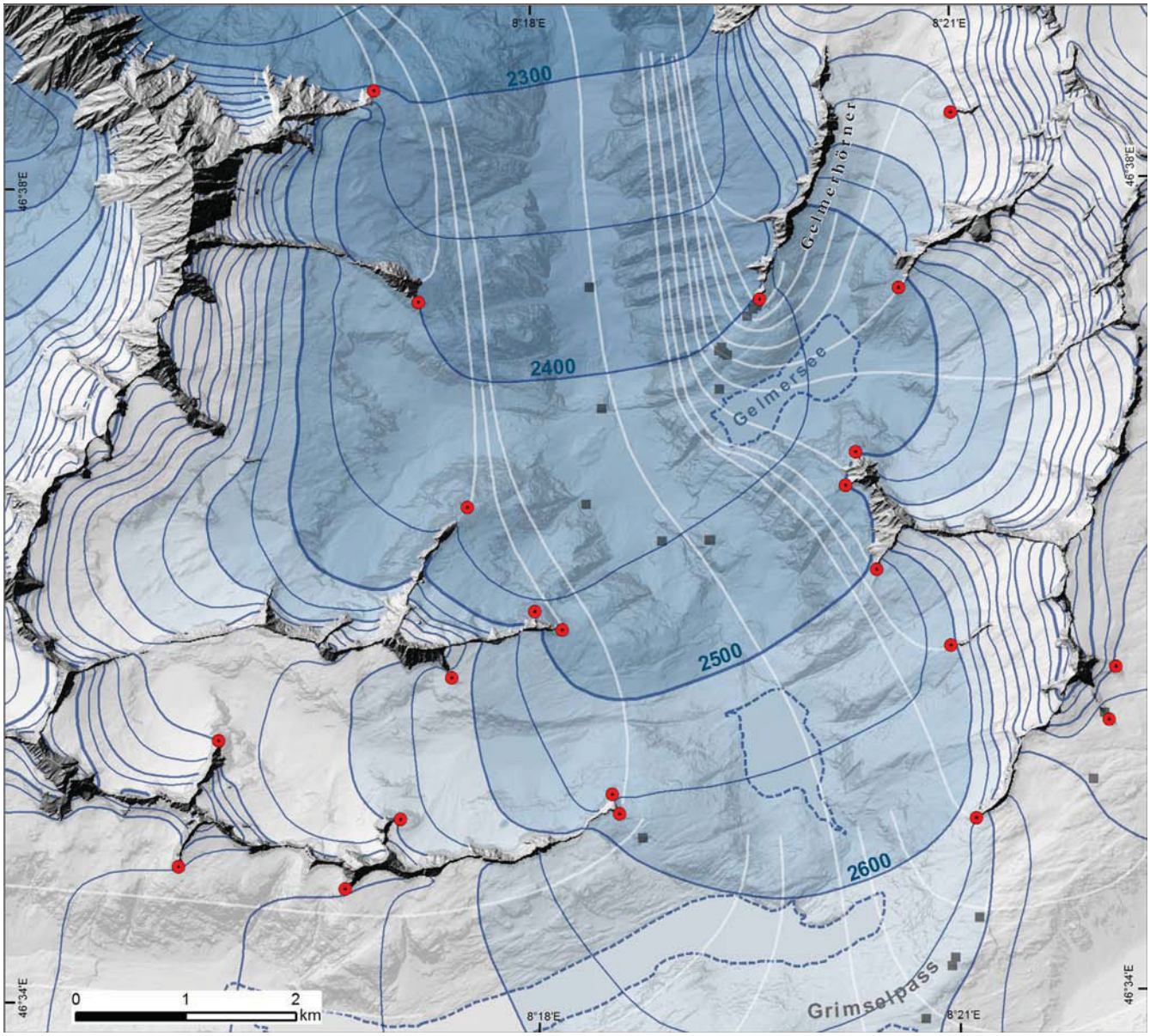

Figure 7. LGM ice surface reconstruction based on trimline elevation points (red dots, Table 1) and glacial erosional marks (Figs 2 and 4). Our reconstruction is generally consistent with the geometry of earlier ones (Jäckli, 1962; Florineth and Schlüchter, 1998; Bini *et al.*, 2009; Fig. 1). It is constrained by a much denser network of trimline elevation points and therefore represents a more detailed model for the study area. Same extent as Fig. 2. Hillshade model in background reproduced by permission of swisstopo (JA100120).

were therefore let down earlier, most likely during lowering of the LGM ice surface and certainly before the Gschnitz readvance at 17–16 ka (Ivy-Ochs *et al.*, 2006a). Yet they apparently have been exposed for >2000 years less. Why? The ages show no correlation to boulder size, which supports our argument for only thin snow cover on the Gelmerhörner ridge. As we see no field evidence for the presence of till, temporary sediment cover of significant thickness can also be excluded, at least on top of GELM3 and 10/11, boulders standing 4 and 5 m tall, respectively. In contrast to the narrow and steep setting where the trimline samples were collected, the Gelmerhörner ridge at the trough shoulder is sufficiently wide and flat to support a small body of ice or firn. We suggest that a patch of remnant ice persisted on the trough shoulder during the early Lateglacial (Fig. 6C). The measured ages mark the point in time when individual boulders assumed a stable position during and after the ice melt some time before the Bølling–Allerød interstadial. While the ice was still present, today's boulder tops were presumably exposed to varying degrees, which would lead to the observed scatter in ages. The conserved glacial marks of the LGM generation on the trough shoulder show that the Lateglacial remnant ice patch was non-eroding, i.e. probably not moving and perhaps even cold-based. Finally, apparently too young ages may reflect spalling or toppling of boulders (Putkonen and Swanson, 2003).

Comparable ages are reported from three nearby sites: earliest signs of deglaciation at Grimsel Pass (Kelly *et al.*, 2006) and at Gotthard Pass (Hippe *et al.*, 2014) are dated to 15.3 ± 0.8 ka (recalculated in Table 3) and 15.9 ± 0.5 ka, respectively. Younger ages at both sites range into the Younger Dryas. Likewise, Albula Pass was deglaciated before 14.1 ± 1.1 ka (Böhlert *et al.*, 2011, sample Alb6, recalculated) and the authors suggest the 'persistence of long-lasting small local ice caps after the breakdown of the LGM ice domes'. Summarizing the observations from these surveys as well as our results, we assume that local patches of ice or firn remained after the LGM in flat, high-altitude settings in the

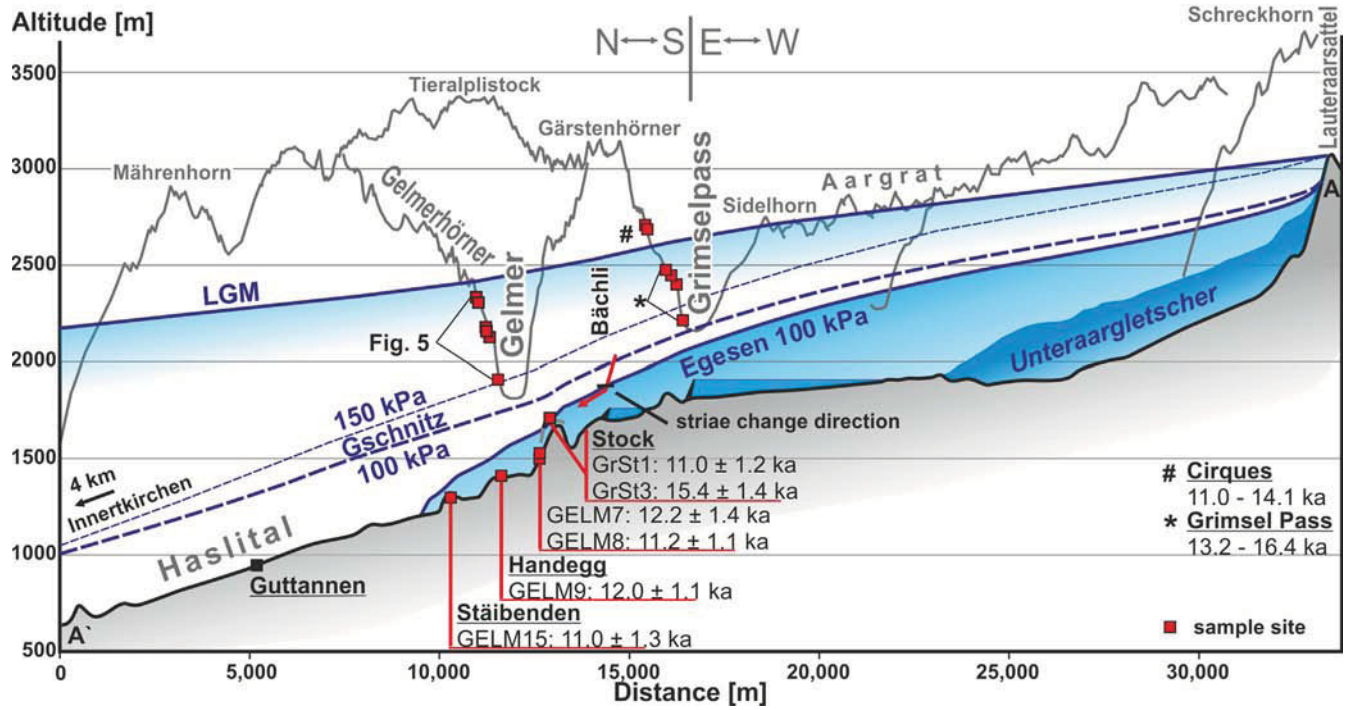

Figure 8. Reconstruction of LGM, Gschnitz and Egesen glacier profiles in the study area and related surface exposure ages. The LGM ice surface follows the trimline elevation points listed in Table 1. For the Gschnitz scenarios depicted here with shear stress values of 100 and 150 kPa moraines near Innertkirchen were chosen as the terminal position using Benn and Hulton (2010); see text for details. The ice surface reaches the sampling sites at the Gelmerhörner trough shoulder in neither case, nor with terminal positions as remote as Lake Brienz ~45 km further downvalley (not shown). The Egesen ice surface is constrained to be just slightly higher than Stock and lower than the directional change of striae at Bächli valley (red arrow), but extended further than GELM15 at Stäibenden (see text). These constraints are met by a model with 100 kPa shear stress and a terminal position not far beyond Stäibenden.

High Alps, such as passes or trough shoulders. They presumably persisted until the Bølling–Allerød interstadial.

Egesen stadial

The Egesen stadial marks the last Lateglacial readvance in the Alps after warm conditions during the Bølling–Allerød interstadial (e.g. Ivy-Ochs *et al.*, 2006b). Our ages indicate that the trough shoulder stayed ice-free throughout the Younger Dryas in contrast to the earlier Lateglacial advances. We did not identify any glacial deposits or landforms in Haslital to constrain the extent of the Egesen glacier. They were possibly buried by the ubiquitous fans deposited by various types of hillslope processes (Kober *et al.*, 2012). Hantke (1980) maps moraines on the bedrock riegel at Handegg (Figs 1 and 2) and correlates them to the Egesen stadial (Hantke, 2011). The ridge consists entirely of glacially polished bedrock now partially covered by vegetation, however. No till or sediments were encountered. The surface exposure ages of our valley samples allow stating a minimum Egesen ice extent. Ranging from 12.2 to 10.8 ka they all conform to complete deglaciation at the end of the Younger Dryas. The glacier tongue must therefore have reached past Stäibenden where GELM15 was collected (Fig. 2).

More information on the Egesen Aare glacier can be extracted from the observed erosional marks. The third generation of glacial marks at Gelmersee shows diverging ice flow on the bedrock step, then points straight downhill from Gelmer valley into Haslital (Fig. 4B, red symbols). This denotes a reorganization of ice-flow patterns where the tributary glacier from Gelmer valley was no longer affected by the glacier in Haslital, but flowed freely downhill. Therefore, the ice surface of the Egesen Aare glacier must have been lower than the bedrock step of the hanging valley at approximately 1800 m. The same argument is valid at the mouth of Bächli valley, where striations record free downhill ice flow until 1920 m (Fig. 2).

The age of the boulder GrSt1 of 11.0 ± 1.2 ka on top of Stock suggests that the bedrock high on the Haslital trough floor was covered by the Aare Egesen glacier. The nearby bedrock surface GrSt3 was exposed for 15.4 ± 1.4 ka, which indicates the opposite. One possible interpretation is that while the boulder GrSt1 was deposited on top of Stock by the Aare Egesen glacier, the ice cover was relatively thin and did not significantly erode the bedrock. This is analogous to the situation at nearby Grueben cirque (Fig. 1), where it was shown that the LIA Grueben glacier polished the bedrock at its lateral ice margin without eroding it deeper than a few centimetres (C. Wirsig *et al.*, unpubl. data).

The elevation of the Egesen ice surface is therefore constrained at several points in the study area. It was below the thresholds of Gelmer valley at 1800 m, Bächli valley at 1920 m and below or just slightly above Stock at 1720 m, but was higher than GELM8 (1522 m) and reached further than GELM15 at Stäibenden. These constraints are met by a model with 100 kPa shear stress and a terminal position not far beyond Stäibenden, certainly upvalley of Guttannen (Fig. 8).

The exposure ages of the valley samples in this study conform well to global climate amelioration at the beginning of the Holocene (e.g. Marcott *et al.*, 2013). Furthermore, they compare remarkably well with the timing of ice retreat from the cirques at nearby Nägelisgrätli (Fig. 2) (Ivy-Ochs, 1996; Ivy-Ochs *et al.*, 2006b, 2007) and Juchlistock (Kelly *et al.*, 2006) of 14.1–11.0 ka (recalculated in Table 3). Likewise, Grimsel Pass was deglaciated at roughly the same time at 13.2 ± 0.8 ka (GP1, recalculated in Table 3; Kelly *et al.*, 2006), as was Gotthard Pass (11.1 ± 0.4 ka;

Hippe *et al.*, 2014). A bedrock ridge in the Grueben cirque that was partially covered by a glacier during the LIA yields only slightly younger exposure ages of 9.7 ± 0.3 ka (C. Wirsig *et al.*, unpubl. data).

Subglacial erosion by the Egesen Aare glacier was notably non-uniform. On the floor of Haslital, except on Stock, bedrock ridges were sufficiently eroded to remove any nuclides accumulated during previous phases of exposure, in particular the Bølling–Allerød interstadial. Similar observations have been made at Nägelisgrätli (Ivy-Ochs *et al.*, 2007) and Gotthard Pass (Hippe *et al.*, 2014). At Gelmersee, however, crescentic gouges of the LGM were overprinted but not erased by the Egesen ice. Subglacial erosion there was clearly limited to a few centimetres at most.

Conclusions

We used a combination of ^{10}Be surface exposure ages, field observations and ice surface models to constrain the evolution of glaciers in the Oberhasli from the LGM to the early Holocene. The ice surfaces that we attribute to three glacial phases – the LGM, Gschnitz and Egesen stadials – were reconstructed. Due to the immediate connection to the Rhône ice dome, results presented here can be extrapolated to a significant part of the Alps.

Haslital was occupied by ice up to the LGM trimline until 23.0 ± 0.8 ka, when presumably the Aare glacier surface initially lowered slightly. Significant retreat occurred no later than 17.7 ± 0.8 ka. Within the uncertainties of the dating methods this is synchronous with or shortly after the deglaciation of the Swiss northern Alpine foreland. As Alpine valleys were ice-free before the Gschnitz readvance, ice decay must have been rapid. We present a hypothesis to explain this rapid ice disappearance, where accumulation zones decrease due to a small increase of the LGM ELA, followed by a decline in shear stress in the long, gently sloped piedmont lobes that leads to a significant deceleration of ice flow. Further work needs to be done to validate this, however.

Nevertheless, the study has demonstrated the challenge in finding target study sites for surface exposure dating with a record of LGM ice surface decay in the High Alps. Like most samples from previous studies, the trough shoulder samples were collected in a flat area within the accumulation zone of Lateglacial stadials. In these situations, however, remnant ice patches probably persisted until the Bølling–Allerød interstadial. Surface exposure ages thus record the disappearance of local ice, not the rate of the LGM ice surface lowering. Future studies are therefore advised to aim either for sharp ridges close to the trimline where ice cannot accumulate, or for lower elevation sites below the Gschnitz ELA, e.g. in the Prealps.

Despite the absence of moraines, the Egesen ice surface of the Aare glacier is well constrained by a combination of the interpretation of glacial erosional marks and surface exposure ages. Ice surface modelling indicates that its terminal position was beyond Stäibenden but upvalley of Guttannen. Deglaciation of the Oberhasli was finally completed 12.2–10.8 ka BP, at the end of the Younger Dryas.

Acknowledgments. This work was funded by the Swiss National Fonds (SNF), project 2-77099-11 to S. Ivy-Ochs and by AGH-UST statutory grant No. 15.11.140.175 to J. Zasadni. We greatly appreciate the support of the whole team at LIP at ETH Zürich. Special thanks to Caroline Welte and Reto Grischott for help in the fieldwork. The thoughtful comments of the editor J. Licciardi, J. Heyman and one anonymous reviewer helped greatly to improve the manuscript.

Abbreviations. AMS, accelerator mass spectrometry; DEM, Digital Elevation Model; ELA, equilibrium line altitude; LGM, Last Glacial Maximum; LIA, Little Ice Age; NENA, north-east North America.

References

Abrecht J. 1994. Geologic units of the Aar massif and their pre-Alpine rock associations: a critical review. *Schweizerische Mineralogische und Petrographische Mitteilungen* **74**: 5–27.

Agassiz L. 1838. On the polished and striated surfaces of the rocks which form the beds of glaciers in the Alps. *Proceedings of the Geological Society London* **3**: 321–322.

Akçar N, Ivy-Ochs S, Kubik PW *et al.* 2011. Post-depositional impacts on "Findlinge" (erratic boulders) and their implications for surface-exposure dating. *Swiss Journal of Geosciences* **104**: 445–453 [DOI: 10.1007/s00015-011-0088-7].

Balco G, Briner J, Finkel RC *et al.* 2009. Regional beryllium-10 production rate calibration for late-glacial northeastern North America. *Quaternary Geochronology* **4**: 93–107 [DOI: 10.1016/j.quageo.2008.09.001].

Balco G, Stone JO, Lifton NA *et al.* 2008. A complete and easily accessible means of calculating surface exposure ages or erosion rates from ^{10}Be and ^{26}Al measurements. *Quaternary Geochronology* **3**: 174–195 [DOI: 10.1016/j.quageo.2007.12.001].

Beck P. 1932. Über den eiszeitlichen Aaregletscher und die Quartärchronologie. *Verein der Naturforschenden Gesellschaft Thun* **113**: 343–359.

Benn DI, Hulton NRJ. 2010. An Excel™ spreadsheet program for reconstructing the surface profile of former mountain glaciers and ice caps. *Computers and Geosciences* **36**: 605–610 [DOI: 10.1016/j.cageo.2009.09.016].

Benn DJ, Evans DJA. 2010. *Glaciers & Glaciation*. Hodder Education: London.

Bini A, Buoncristiani JF, Couterrand S, *et al.* 2009. *Switzerland during the Last Glacial Maximum 1: 500,000*. Bundesamt für Landestopografie swisstopo.

Böhlert R, Egli M, Maisch M *et al.* 2011. Application of a combination of dating techniques to reconstruct the Lateglacial and early Holocene landscape history of the Albula region (eastern Switzerland). *Geomorphology* **127**: 1–13 [DOI: 10.1016/j.geomorph.2010.10.034].

Bond G, Heinrich H, Broecker W *et al.* 1992. Evidence for massive discharge of icebergs into the North Atlantic Ocean during the last glacial period. *Nature* **360**: 245–249 [DOI: 10.1038/360245a0].

Briner JP, Young NE, Goehring BM *et al.* 2012. Constraining Holocene ^{10}Be production rates in Greenland. *Journal of Quaternary Science* **27**: 2–6 [DOI: 10.1002/jqs.1562].

Christl M, Vockenhuber C, Kubik PW *et al.* 2013. The ETH Zürich AMS facilities: performance parameters and reference materials. *Nuclear Instruments and Methods in Physics Research, Section B: Beam Interactions with Materials and Atoms* **294**: 29–38 [DOI: 10.1016/j.nimb.2012.03.004].

Clark PU, Shakun JD, Baker PA *et al.* 2012. Global climate evolution during the last deglaciation. *Proceedings of the National Academy of Sciences of the United States of America* **109**: E1134–E1142 [DOI: 10.1073/pnas.1116619109] [PubMed: 22331892].

Claude A, Ivy-Ochs S, Kober F *et al.* 2014. The Chironico landslide (Valle Leventina, southern Swiss Alps): age and evolution. *Swiss Journal of Geosciences* **107**: 273–291 [DOI: 10.1007/s00015-014-0170-z].

Cuffey KM, Paterson WSB. 2010. *The Physics of Glaciers*. Elsevier: Amsterdam.

Delunel R, Bourlès DL, van der Beek PA *et al.* 2014. Snow shielding factors for cosmogenic nuclide dating inferred from long-term neutron detector monitoring. *Quaternary Geochronology* **24**: 16–26 [DOI: 10.1016/j.quageo.2014.07.003].

Dielforder A, Hetzel R. 2014. The deglaciation history of the Simplon region (southern Swiss Alps) constrained by ^{10}Be exposure dating of ice-molded bedrock surfaces. *Quaternary Science Reviews* **84**: 26–38 [DOI: 10.1016/j.quascirev.2013.11.008].

Dühnforth M, Anderson RS, Ward D *et al.* 2010. Bedrock fracture control of glacial erosion processes and rates. *Geology* **38**: 423–426 [DOI: 10.1130/G30576.1].

Dunai TJ, Binnie SA, Hein AS *et al*. 2014. The effects of a hydrogen-rich ground cover on cosmogenic thermal neutrons: implications for exposure dating. *Quaternary Geochronology* **22**: 183–191 [DOI: 10.1016/j.quageo.2013.01.001].

Ehlers J, Gibbard PL, Hughes PD. 2011. *Quaternary Glaciations – Extent and Chronology: a Closer Look*. Elsevier: Amsterdam.

Fabel D, Harbor J, Dahms D *et al*. 2004. Spatial patterns of glacial erosion at a valley scale derived from terrestrial cosmogenic ^{10}Be and ^{26}Al concentrations in rock. *Annals of the Association of American Geographers* **94**: 241–255 [DOI: 10.1111/j.1467-8306.2004.09402001.x].

Fabel D, Stroeven AP, Harbor J *et al*. 2002. Landscape preservation under Fennoscandian ice sheets determined from in situ produced ^{10}Be and ^{26}Al. *Earth and Planetary Science Letters* **201**: 397–406 [DOI: 10.1016/S0012-821X(02)00714-8].

Farinotti D, Huss M, Bauder A *et al*. 2009. A method to estimate the ice volume and ice-thickness distribution of alpine glaciers. *Journal of Glaciology* **55**: 422–430 [DOI: 10.3189/002214309788816759].

Federici PR, Granger DE, Ribolini A *et al*. 2012. Last Glacial Maximum and the Gschnitz stadial in the Maritime Alps according to ^{10}Be cosmogenic dating. *Boreas* **41**: 277–291 [DOI: 10.1111/j.1502-3885.2011.00233.x].

Fenton CR, Hermanns RL, Blikra LH *et al*. 2011. Regional ^{10}Be production rate calibration for the past 12 ka deduced from the radiocarbon-dated Grotlandsura and Russenes rock avalanches at 69°N, Norway. *Quaternary Geochronology* **6**: 437–452 [DOI: 10.1016/j.quageo.2011.04.005].

Florineth D, Schlüchter C. 1998. Reconstructing the Last Glacial Maximum (LGM) ice surface geometry and flowlines in the Central Swiss Alps. *Eclogae Geologicae Helvetiae* **91**: 391–407.

Gianotti F, Forno MG, Ivy-Ochs S, *et al*. 2015. Stratigraphy of the Ivrea Morainic Amphitheatre (NW Italy): an updated Synthesis. *Alpine and Mediterranean Quaternary* **28**: 29–58.

Gianotti F, Forno MG, Ivy-Ochs S *et al*. 2008. New chronological and stratigraphical data on the Ivrea amphitheatre (Piedmont, NW Italy). *Quaternary International* **190**: 123–135 [DOI: 10.1016/j.quaint.2008.03.001].

Glasser NF, Bennett MR. 2004. Glacial erosional landforms: origins and significance for palaeoglaciology. *Progress in Physical Geography* **28**: 43–75 [DOI: 10.1191/0309133304pp401ra].

Goehring BM, Lohne ØS, Mangerud J *et al*. 2012. Late glacial and Holocene ^{10}Be production rates for western Norway. *Journal of Quaternary Science* **27**: 89–96 [DOI: 10.1002/jqs.1517].

Gosse JC, Phillips FM. 2001. Terrestrial in situ cosmogenic nuclides: theory and application. *Quaternary Science Reviews* **20**: 1475–1560 [DOI: 10.1016/S0277-3791(00)00171-2].

Hadorn P, Thew N, Coope GR *et al*. 2002. A Late-Glacial and early Holocene environment and timing of retreat of the Reuss Glacier climate history for the Neuchâtel region (CH). In *Equilibres et Ruptures dans les Ecosystèmes depuis 20 000 ans en Europe de l'Ouest*, Richard H, Vignot A (eds). Presses Universitaires de Franche-Comté: Besançon; 75–90.

Hantke R. 1980. *Eiszeitalter*. Ott Verlag: Thun.

Hantke R. 2011. *Eiszeitalter*. hep Verlag ag: Bern.

Heyman J. 2014. Paleoglaciation of the Tibetan Plateau and surrounding mountains based on exposure ages and ELA depression estimates. *Quaternary Science Reviews* **91**: 30–41 [DOI: 10.1016/j.quascirev.2014.03.018].

Hippe K, Ivy-Ochs S, Kober F *et al*. 2014. Chronology of Lateglacial ice flow reorganization and deglaciation in the Gotthard Pass area, Central Swiss Alps, based on cosmogenic ^{10}Be and in situ ^{14}C. *Quaternary Geochronology* **19**: 14–26 [DOI: 10.1016/j.quageo.2013.03.003].

Jäckli H. 1962. Die Vergletscherung der Schweiz im Würmmaximum. *Eclogae Geologicae Helvetiae* **55**(2).

Penck A, Brückner E. 1901/9. *Die Alpen im Eiszeitalter*. Tauchitz: Leipzig.

Ivy-Ochs S. 1996. *The dating of rock surfaces using in situ produced ^{10}Be, ^{26}Al and 36Cl, with examples from Antarctica and the Swiss Alps*. PhD thesis, ETH Zürich.

Ivy-Ochs S. 2015. Glacier variations in the European Alps at the end of the last glaciation. *Cuadernos de Investigación Geográfica* **41**: 295–315 [DOI: 10.18172/cig.2750].

Ivy-Ochs S, Kerschner H, Kubik PW *et al*. 2006a. Glacier response in the European Alps to Heinrich Event 1 cooling: the Gschnitz stadial. *Journal of Quaternary Science* **21**: 115–130 [DOI: 10.1002/jqs.955].

Ivy-Ochs S, Kerschner H, Maisch M *et al*. 2009. Latest Pleistocene and Holocene glacier variations in the European Alps. *Quaternary Science Reviews* **28**: 2137–2149 [DOI: 10.1016/j.quascirev.2009.03.009].

Ivy-Ochs S, Kerschner H, Reuther A *et al*. 2006b. The timing of glacier advances in the northern European Alps based on surface exposure dating with cosmogenic ^{10}Be, ^{26}Al, ^{36}Cl and ^{21}Ne. *Geological Society of America Special Paper* **415**: 43–60.

Ivy-Ochs S, Kerschner H, Reuther A *et al*. 2008. Chronology of the last glacial cycle in the European Alps. *Journal of Quaternary Science* **23**: 559–573 [DOI: 10.1002/jqs.1202].

Ivy-Ochs S, Kerschner H, Schlüchter C. 2007. Cosmogenic nuclides and the dating of Lateglacial and Early Holocene glacier variations: the Alpine perspective. *Quaternary International* **164–165**: 53–63 [DOI: 10.1016/j.quaint.2006.12.008].

Ivy-Ochs S, Schäfer J, Kubik PW *et al*. 2004. Timing of deglaciation on the northern Alpine foreland (Switzerland). *Eclogae Geologicae Helvetiae* **97**: 47–55 [DOI: 10.1007/s00015-004-1110-0].

Keller O, Krayss E. 2005. Der Rhein-Linth-Gletscher im letzten Hochglazial. *Vierteljahrsschrift der Naturforschenden Gesellschaft in Zürich* **150**: 69–85.

Kelly MA, Buoncristiani JF, Schlüchter C. 2004. A reconstruction of the last glacial maximum (LGM) ice-surface geometry in the western Swiss Alps and contiguous Alpine regions in Italy and France. *Eclogae Geologicae Helvetiae* **97**: 57–75 [DOI: 10.1007/s00015-004-1109-6].

Kelly M, Ivy-Ochs S, Kubik P *et al*. 2006. Chronology of deglaciation based on ^{10}Be dates of glacial erosional features in the Grimsel Pass region, central Swiss Alps. *Boreas* **35**: 634–643 [DOI: 10.1080/03009480600690829].

Kerschner H, Berktold E. 1982. Spätglaziale Gletscherstände und Schuttformen im Senderstal, nördliche Stubaier Alpen, Tirol. *Zeitschrift für Gletscherkunde und Glazialgeologie* **17**: 125–134.

Kober F, Hippe K, Salcher B *et al*. 2012. Debris-flow-dependent variation of cosmogenically derived catchment-wide denudation rates. *Geology* **40**: 935–938 [DOI: 10.1130/G33406.1].

Kohl CP, Nishiizumi K. 1992. Chemical isolation of quartz for measurement of in-situ-produced cosmogenic nuclides. *Geochimica et Cosmochimica Acta* **56**: 3583–3587 [DOI: 10.1016/0016-7037(92)90401-4].

Labhart TP. 1977. *Aarmassiv und Gotthardmassiv*. Gebruder Borntraeger Verlagsbuchhandlung; Stuttgart.

Lal D. 1991. Cosmic ray labeling of erosion surfaces: in situ nuclide production rates and erosion models. *Earth and Planetary Science Letters* **104**: 424–439 [DOI: 10.1016/0012-821X(91)90220-C].

Lister GS. 1988. A 15,000-year isotopic record from Lake Zürich of deglaciation and climatic change in Switzerland. *Quaternary Research* **29**: 129–141 [DOI: 10.1016/0033-5894(88)90056-7].

Maisch M. 1982. Zur Gletscher- und Klimageschichte des alpinen Spätglazials. *Geographica Helvetica* **37**: 93–104 [DOI: 10.5194/gh-37-93-1982].

Maisch M, Wipf A, Denneler B *et al*. 1999 *Die Gletscher der Schweizer Alpen. Gletscherhochstand 1850, Aktuelle Vergletscherung, Gletscherschwund-Szenarien*. vdf Hochschulverlag ETH Zürich.

Marcott SA, Shakun JD, Clark PU *et al*. 2013. A reconstruction of regional and global temperature for the past 11,300 years. *Science (New York, N.Y.)* **339**: 1198–1201 [DOI: 10.1126/science.1228026] [PubMed: 23471405].

Mayr F, Heuberger H. 1968. Type areas of Lateglacial and postglacial deposits in Tyrol, Eastern Alps. *Proceeding VII INQUA Congress* **14**: 143–165.

Monegato G, Ravazzi C, Donegana M *et al*. 2007. Evidence of a two-fold glacial advance during the last glacial maximum in the Tagliamento end moraine system (eastern Alps). *Quaternary Research* **68**: 284–302 [DOI: 10.1016/j.yqres.2007.07.002].

Nishiizumi K, Imamura M, Caffee MW *et al*. 2007. Absolute calibration of ^{10}Be AMS standards. *Nuclear Instruments and Methods in Physics Research, Section B: Beam Interactions with*

Materials and Atoms **258**: 403–413 [DOI: 10.1016/j.nimb.2007.01.297].

Preusser F, Graf HR, Keller O, Krayss E, Schlüchter C. 2011. Quaternary glaciation history of northern Switzerland. *Quaternary Science Journal* **60**: 282–305.

Putkonen J, Swanson T. 2003. Accuracy of cosmogenic ages for moraines. *Quaternary Research* **59**: 255–261 [DOI: 10.1016/S0033-5894(03)00006-1].

Putnam AE, Schaefer JM, Denton GH *et al*. 2012. Regional climate control of glaciers in New Zealand and Europe during the pre-industrial Holocene. *Nature Geoscience* **5**: 627–630 [DOI: 10.1038/ngeo1548].

Ravazzi C, Pini R, Badino F *et al*. 2014. The latest LGM culmination of the Garda Glacier (Italian Alps) and the onset of glacial termination. Age of glacial collapse and vegetation chronosequence. *Quaternary Science Reviews* **105**: 26–47 [DOI: 10.1016/j.quascirev.2014.09.014].

Reber R, Akçar N, Ivy-Ochs S *et al*. 2014. Timing of retreat of the Reuss Glacier (Switzerland) at the end of the Last Glacial Maximum. *Swiss Journal of Geosciences* **107**: 293–307 [DOI: 10.1007/s00015-014-0169-5].

Reitner JM. 2007. Glacial dynamics at the beginning of Termination I in the Eastern Alps and their stratigraphic implications. *Quaternary International* **164–165**: 64–84 [DOI: 10.1016/j.quaint.2006.12.016].

Reuther A, Fiebig M, Ivy-Ochs S *et al*. 2011. Deglaciation of a large piedmont lobe glacier in comparison with a small mountain glacier – new insight from surface exposure dating. Two studies from SE Germany. *Quaternary Science Journal* **60**: 248–269.

Schildgen TF, Phillips WM, Purves RS. 2005. Simulation of snow shielding corrections for cosmogenic nuclide surface exposure studies. *Geomorphology* **64**: 67–85 [DOI: 10.1016/j.geomorph.2004.05.003].

Schindelwig I, Akçar N, Kubik PW *et al*. 2012. Lateglacial and early Holocene dynamics of adjacent valley glaciers in the Western Swiss Alps. *Journal of Quaternary Science* **27**: 114–124 [DOI: 10.1002/jqs.1523].

Solomina ON, Bradley RS, Hodgson DA *et al*. 2015. Holocene glacier fluctuations. *Quaternary Science Reviews* **111**: 9–34 [DOI: 10.1016/j.quascirev.2014.11.018].

Stroeven AP, Fabel D, Harbor J *et al*. 2002. Quantifying the erosional impact of the Fennoscandian Ice Sheet in the Torneträsk-Narvik Corridor, northern Sweden, based on cosmogenic radionuclide data. *Geografiska Annaler, Series A: Physical Geography* **84**: 275–287 [DOI: 10.1111/j.0435-3676.2002.00182.x].

Thorp PW. 1981. A trimline method for defining the upper limit of Loch Lomond Advance glaciers: examples from the Loch Levan and Glencoe areas. *Scottish Journal of Geology* **17**: 49–64.

van Husen D. 1977. Zur Fazies und Stratigraphie der jungpleistozänen Ablagerungen im Trauntal (mit Quartärgeologischer Karte). *Jahrbuch der Geologischen Bundesanstalt* **120**: 1–130.

van Husen D. 1987. *Die Ostalpen in den Eiszeiten*. Verlag der geologischen Bundesanstalt.

van Husen D. 1997. LGM and late-glacial fluctuations in the Eastern Alps. *Quaternary International* **38–39**: 109–118.

Young NE, Schaefer JM, Briner JP *et al*. 2013. A ^{10}Be production-rate calibration for the Arctic. *Journal of Quaternary Science* **28**: 515–526 [DOI: 10.1002/jqs.2642].

Zweck C, Zreda M, Desilets D. 2013. Snow shielding factors for cosmogenic nuclide dating inferred from Monte Carlo neutron transport simulations. *Earth and Planetary Science Letters* **379**: 64–71 [DOI: 10.1016/j.epsl.2013.07.023].